ACS APPLIED MATERIALS & INTERFACES

Letter

www.acsami.org

# Enhanced Performance of Organic Thin Film Solar Cells Using Electrodes with Nanoimprinted Light-Diffraction and Light-Diffusion Structures

Jheng-Yuan Chen,[†] Ming-Hung Yu,[†] Chih-Yu Chang,[†] Yi-Hsiang Chao,[†] Kien Wen Sun,*[,†,‡] and Chain-Shu Hsu[†]

[†]Department of Applied Chemistry, National Chiao Tung University, 1001 University Road, Hsinchu 30010, Taiwan

[‡]Department of Electronics Engineering and Institute of Electronics Engineering, National Chiao Tung University, 1001 University Road, Hsinchu 30010, Taiwan

**ABSTRACT:** An ITO substrate with periodic surface nanostructures was used to induce strong diffusion and diffraction of incident light. The nanostructures were fabricated using nanoimprint lithography on photoresist followed by coating of the ITO layer and organic materials with uniform morphology. The nanostructures embedded into the ITO layer were found to increase absorption in poly(3-hexylthiophene) : [6,6]-phenyl-C61-butyric acid methyl ester solar devices. The short-circuit current of the nanostructured organic solar cells improved from 7.07 to 10.76 mA/cm$^2$. This improvement was due to the increased effective optical path of absorbed light resulting from the trapping and scattering by the nanostructures.

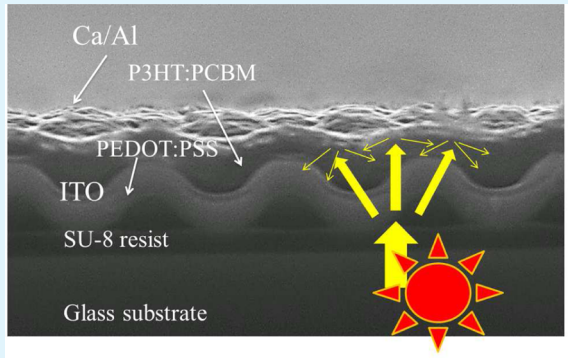


**KEYWORDS:** *nanostructure, nanoimprint lithography, light trapping, organic photovoltaic, diffraction, haze*

Photovoltaic technology enables the direct harvesting of solar energy and is being increasingly recognized as an important component of future global energy production. Among existing solar cells, organic photovoltaics (OPVs) are an attractive paradigm because of their low manufacturing cost, amenability to flexible substrates, and semi-transparency for wide applications. OPVs have recently gained momentum with the continuous development of new organic materials that have pushed the boundary of OPV power conversion efficiencies (PCEs) to >7%.[1−3] OPV devices consisting of a blend of donor and acceptor as a bulk heterojunction (BHJ) active layer are research hotspots. The active layer components are spontaneously phase separated into interconnected domains, and the photocurrent is due to a split of photogenerated excitons at the donor−acceptor heterojunction interface. Free charge carriers are transported through the interconnected domains and collected by the electrodes. The performance of OPVs is limited by two critical factors: short exciton diffusion length (∼10 nm) and low mobility of charge carriers, especially hole mobility within the photoactive layer. BHJ improved PCE because of the nanoscale nature of phase separation that provides a large donor−acceptor interface to allow efficient exciton dissociation. However, a mismatch in length scale between optical absorption and charge transport exists because the thickness of photoactive layer is limited by the low carrier mobility. Typically, the PCE of OPV is limited because of the weak absorbance of the thin photoactive layer in the solar spectrum range. To solve this problem, the thickness of the active layer should be increased for better absorption of the incoming photons. However, a thick active layer increases the series resistance of the device as a result of the limited charge-carrier mobility of the polymers. Therefore, techniques must be developed for efficient optical absorption in films thinner than the optical absorption depth. Thus, surface structures such as periodic patterns or rough surfaces can increase the effective optical path of incident light inside absorbing materials by light trapping or scattering.

The use of nanoscale surface structures for enhancing the light absorption of thin film devices is a more promising method[4,5] than the traditional microscale texturing for crystalline silicon (Si) solar cells. Nanoscale surface structures such as nanowires,[6] nanorods,[7] and nanocones[8] provide enhanced absorption properties by anti-reflective and light scattering effects, as well as a large area for charge separation and radial junction architecture. Nanoscale surface structures are widely used in solar cells such as anti-reflective coatings,[9] crystalline Si solar cells,[6,7] thin-film solar cell,[8] and hybrid solar cells[10,11] because of the above-mentioned advantages. In organic solar cells, nanostructures are incorporated into device morphologies, including transparent electrodes,[12−15] hole injection layers,[16−19] and active layers.[20−25] Textured electrodes can reportedly provide efficient light trapping to increase the

**Received:** December 19, 2013
**Accepted:** April 15, 2014
**Published:** April 15, 2014

   dx.doi.org/10.1021/am405865w | *ACS Appl. Mater. Interfaces* 2014, 6, 6164−6169

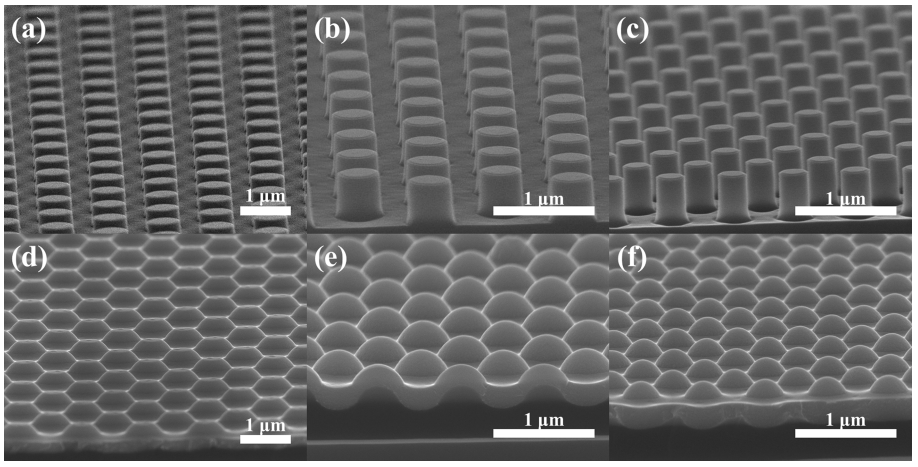


**Figure 1.** SEM images of the Si molds with structure periods of (a) 1200, (b) 800, and (c) 600 nm and the imprint results with ITO deposition on structures with periods of (d) 1200, (e) 800, and (f) 600 nm.

optical path of light and to enhance OPV efficiency.[12,14] The improvement in performance is also attributed to optical effects, predominantly angular and diffuse reflection from the curved and periodic back reflector. By structuring the hole injection and photoactive layers, the effective optical path and the interfacial area can be increased, thereby leading to better molecular chain alignment and a relatively short route for holes to reach the anode. Consequently, effective hole mobility and charge carrier collection increase.[16−25]

Nanostructures can be fabricated by various techniques that involve lithography and etching. Versatile techniques such as nanoimprint lithography (NIL) have recently emerged as promising candidates for fabricating nanostructures.[26,27] NIL is a high throughput, high-resolution parallel patterning method in which a surface pattern of a stamp is replicated into a material by mechanical contact and three-dimensional material displacement. The method requires only a simple equipment setup and is thus low cost. In this study, instead of directly embossing nanostructures on the hole injection or photoactive layers, an OPV device was prepared on a nanostructured ITO template to avoid the degradation of OPV performance. The entire process did not require any annealing steps and posed no contamination concerns to the active layer. Previous attempts to deposit organic materials on textured surfaces have led to the overfilling of valleys and shunts at crests,[28] especially for spin-coating processes.[11,12] Improved methods were used in the current work to further modify structures into a wavy profile with a continuous gradient. Both planar and nanostructured OPV devices based on poly(3-hexylthiophene):[6,6]-phenyl-C61-butyric acid methyl ester (P3HT:PCBM) were fabricated to study the influence of periodic nanostructures on OPV performance by optical and electrical characterization.

Si molds were placed in a closed bottle filled with vaporized 1H,1H,2H,2H-perfluoro-octyltrichlorosilane at 250 °C for 1 h. This mold release agent can facilitate the separation of replicas from Si molds when coated onto the surface. To duplicate the mold into polydimethylsiloxane (PDMS, Sylgard 184), PDMS was first mixed with its curing agent at a ratio of 10:1. The Si mold was then immersed in a flat-bottom container filled with PDMS mixtures to a height of 2 mm. After degassing, the container was cured at 60°C for 12 h. The duplicated PDMS mold was directly peeled off from the master mold. To structure SU-8 (MicroChemicals) by nanoimprint, onto which ITO will be deposited, the SU-8 photoresist was first diluted to a concentration with 6.4% solids and then spin-coated on a clean glass substrate at 3000 rpm. The nanostructures were patterned with the commonly used photoresist SU-8 on glass substrates. SU-8 has the advantages of high transparency in the visible wavelength region and was stable at high temperature (>200 °C). Furthermore, the device fabrication can be directly processed with the structured polymer layers on glass without going through any etching process. The SU-8 photoresist is thermoplastic and has a low glass transition temperature (< 50 °C). Before UV curing, the as-prepared substrate covered with SU-8 was imprinted with the PDMS mold using a home-made nanoimprintor at 70°C under 1atm for 1 min. After the PDMS mold was completely filled by the SU-8 photoresist, the sample was exposed to a Xe lamp for 90 s for curing. To further smooth out the structures, the imprinted substrate was then spin coated with a photoresist of a lower concentration (4.5% solids) and exposed for 60 s. Finally, we deposited a layer of ITO onto the structured surface with an RF sputter system to make a conductive and transparent substrate with periodic surface nanostructures.

The device structures for the OPV was ITO/PEDOT:PSS/P3HT:$PC_{61}BM$/Ca/Al. The ITO glass substrates were cleaned with detergent, deionized water, acetone, and isopropyl alcohol in an ultrasonic bath and then dried overnight in an oven at >100 °C. Substrates were covered by PEDOT:PSS (40 nm, Al 4083 provided by H. C. Stark) using spin-coating, and dried in glove box at 150 °C for 30 min. P3HT were dissolved in ODCB (2 wt %), and $PC_{61}BM$ (purchased from Nano-C) was then added into the solution to reach the desired weight ratio. The solution was stirred at 70 °C for overnight and filtrated through a 0.45 $\mu$m filter. In a glove box, the polymer solution was spin-coated at 600 rpm for 40 s onto the PEODOT:PSS-coated substrate with the thickness 180 nm. The devices were solvent annealed with ODCB for 30 min in a Petri dish and then annealed at 150 °C for 15 min. The cathode made of calcium (35 nm) and aluminum (100 nm) was evaporated through a shadow mask under vacuum (<$1 \times 10^{-6}$ Torr). Each sample consists of four independent pixels with active area of 0.04 $cm^2$ defined by the overlap between the underlying ITO and the top electrode. During the characterization, the active area was isolated through a mask. The devices were encapsulated and characterized in air under 100 $mW/cm^2$ AM 1.5 simulated light measurement (Yamashita Denso solar simulator). Current−voltage ($J$−$V$) characteristics of OPV

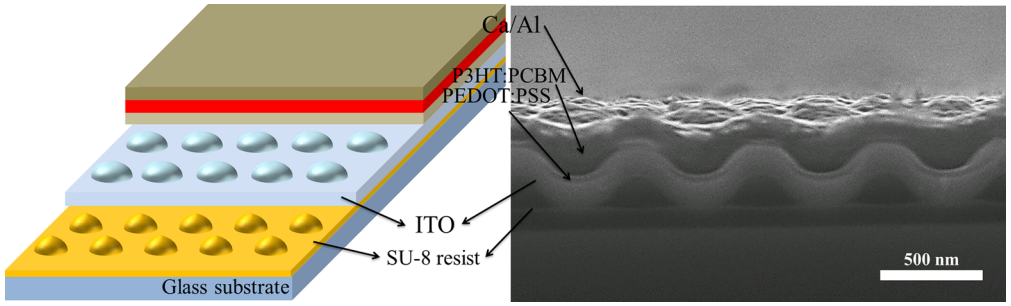


**Figure 2.** Schematic of the nanostructured substrate and the corresponding cross-section SEM image of the as prepared P3HT:PCBM solar cell.

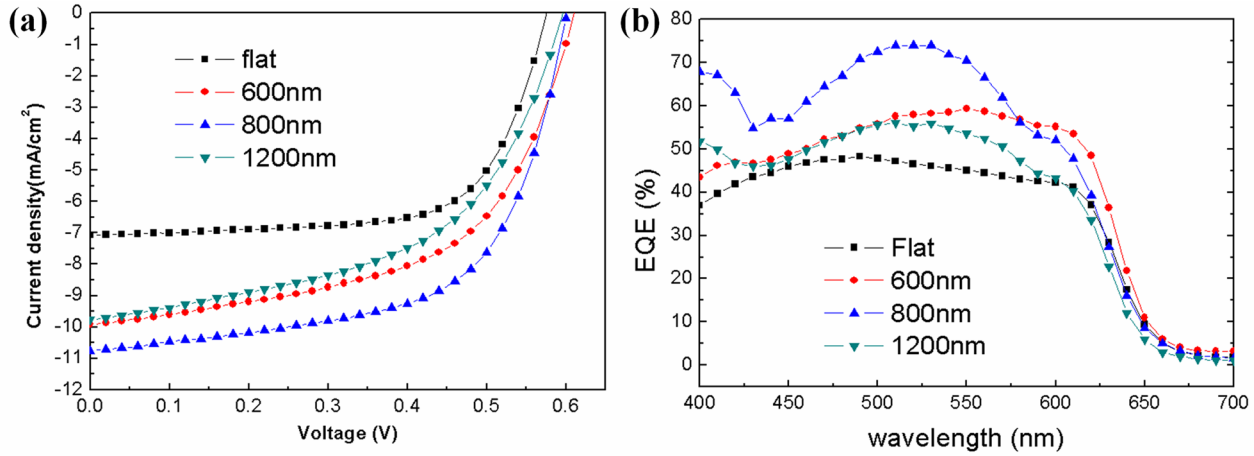


**Figure 3.** (a) Current density−voltage ($J$−$V$) characteristics and (b) external quantum efficiency (EQE) spectra of the OPVs prepared on structured surface of different periods. Results from devices built on flat surface are also displayed for comparison.

devices were obtained by a Keithley 2400 SMU. Solar illumination conforming the JIS Class AAA was provided by a SAN-EI 300W solar simulator equipped with an AM 1.5G filter. The light intensity was calibrated with a Hamamatsu S1336-5BK silicon photodiode. The external quantum efficiency (EQE) measurement was performed by a system combining xenon lamp, a monochromator, a chopper and a lock-in amplifier together with a calibrated silicon photodetector. The device prepared on the nanostructured template followed the same procedures as the device made on the flat surface. All of the geometrical parameters for the nanostructured solar cells were kept the same as the planar solar cells, especially the volume of the active layer.

Patterns on the Si mold were duplicated onto a soft and flexible PDMS mold by cast molding to imprint the structures by UV curing. PDMS was used as standard mold material because of its favorable properties, including elastomeric character, low cost, high optically transparency, low surface energy, and easy molding. If both the mold and substrate were rigid, a high risk would exist because the contact between the mold and substrate would not be uniform. The substrate could also be damaged because of unexpected surface protrusions, such as defects. Therefore, the PDMS flexible mold was chosen to overcome the above problems encountered with a rigid mold. The nanostructures on the PDMS molds were completely reproduced from the Si master molds. Figure 1a−c shows the scanning electron microscopy (SEM) images of the Si molds with periods of 1200, 800, and 600 nm, respectively. All structures formed two-dimensional hexagonal pillar arrays with a height of 400 nm. However, the vertical side profile of the structures did not favor the follow-up physical deposition and spin-coating processes of organic materials because the overfill between pillars impeded the deposition of more uniform organic films. Therefore, the imprinting temperature was increased to improve the filling of the photoresist SU-8 on the PDMS mold. After imprint, the sample was coated again with SU-8 to further smoothen the surface morphology. Figure 1d−f show the SEM images of the imprinted nanostructures with different periods after ITO layer deposition. The modified surface morphology resembled dome-shape structures with a wavy side profile. Assuming anisotropic deposition of the polymeric layers upon OPVs formation, a not too high aspect ratio of the surface structure while keeping the conformal coverage of deposited material within a reasonable range and avoiding steep surface slopes can have noticeable optical effects.

Figure 2 displays the schematic of the organic solar cell device and a cross-section SEM image of the as-prepared device. A transparent conducting oxide layer (ITO in this study) was sputtered on the SU-8 surface to take advantage of the effects of periodic surface nanostructures on the OPVs. As shown in Figure 2, although the spin-coated polymer layer slightly smoothed out the ITO surface, the surface structures remained intact and transferred onto the organic layer. The periodic surface structures were not only safely transferred to the polymer layers but also to the metal layers. Therefore, a uniform and conformal polymer layer following the morphology of the structured substrate was realized. Notably, no shuntlike defects appeared in the SEM image shown in Figure 2.

Figure 3a shows the current density-voltage ($J$−$V$) characteristics of the OPVs prepared on a flat surface and structured surfaces of different periods. Instead of undergoing high-


dx.doi.org/10.1021/am405865w | ACS Appl. Mater. Interfaces 2014, 6, 6164−6169

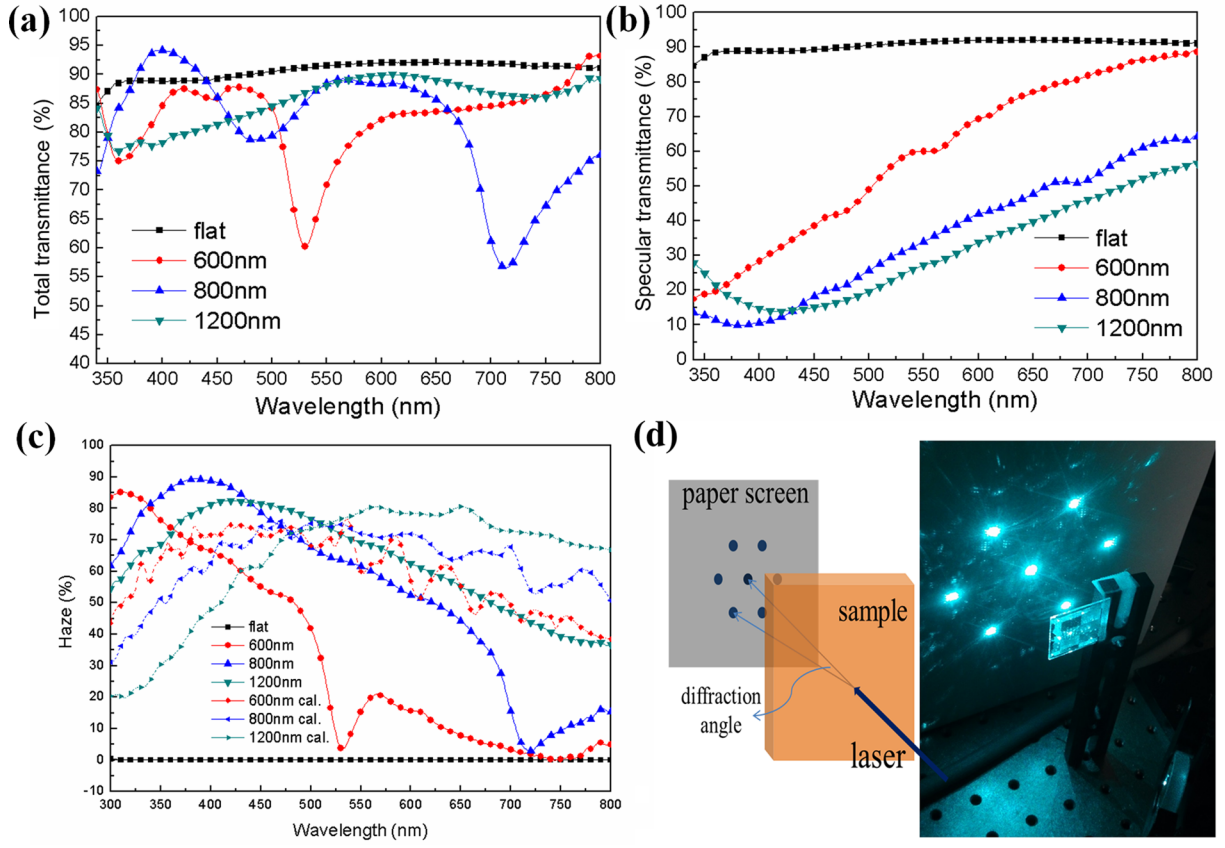


**Figure 4.** (a) Total transmittance spectra, (b) specular transmittance spectra, and (c) haze factors of nanostructured surface with different periods. Results from devices built on flat surface and the calculated haze factors (dash curves) by assuming a polymer layer with a refractive index of 2.0 deposited on the patterned ITO electrode, are also displayed for comparison. (d) Schematic of the diffraction angle measurement setup and the photo image of transmitted diffraction pattern of the structured surface with the 1200 nm period.

temperature post-annealing processes, the ITO layer was deposited at room temperature. Consequently, lower transparency and photocurrent ensued. Therefore, the performance of our reference OPV device was not as good as the device in a previous report.[29] Nevertheless, under the same experimental conditions, devices with periodic surface nanostructures increased in both short circuit current density ($J_{sc}$) and power conversion efficiency (PCE) compared with the reference cell, which indicated that the nanostructures caused increased light absorption. The optimum cell performance was achieved on a device with a structure period of 800 nm. Our best result showed increased $J_{sc}$ from 7.07 to 10.76 mA/cm$^2$ and increased PCE from 2.75 to 3.92%, respectively. To investigate the light-trapping nature of the devices with surface nanostructures, we performed external quantum efficiency (EQE) measurements on devices with structures of different periods (Figure 3b). The flat-surface device showed an EQE below 50% throughout the entire polymer absorption wavelength region. With the surface nanostructures, EQE uniformly increased by different degrees depending on the structure periods. Figure 3(b) shows that the device with the 800 nm period gave the best performance in EQE, particularly in the 450−600 nm wavelength region.

To study the optical effects of the nanostructured surface with different periods, we measured the total transmittance of the glass substrates coated with the structured SU-8 resist. The spectra shown in Figure 4a were measured using an UV/visible/NIR spectrophotometer (Hitachi U-4100) equipped with an integrating sphere with the incoming light entered from the glass side. Several distinct dips were observed for structures with 600 and 800 nm periods. The total transmittance spectra within the measured ranges were strongly modified by the diffraction of samples with structure periods of 600 and 800 nm compared with the 1200 nm and the flat one. Taking the sample with the structure period of 800 nm as an example, the first- and second-order diffractions occurred between 400 and 600 nm. As the wavelength moved from 400 nm toward longer ones, the second-order diffraction light gradually entered the total internal reflection mode because of the increase in diffraction angles, which resulted in the first minimum transmission at ∼475 nm. Only first-order diffraction light existed as the wavelength moved beyond 600 nm. The first-order diffraction light entered the total internal reflection mode again with increased wavelength, which resulted in the second minimum transmission at ∼715 nm. The wavelengths where the transmission dips (total internal reflection) occurred shifted toward shorter and longer wavelengths as the periods of the structures were decreased or increased, respectively.

The results in Figure 4a show that periodic surface structures provided light diffraction with increased diffraction angles as the periods were reduced (at a fixed wavelength) and as the wavelengths were increased (at a fixed period). To clarify the diffraction effect, the specular transmittance (Figure 4b) that eliminated indirect (diffuse) transmittance was measured. The corresponding haze factor (haze = $(T_{total} - T_{specular})/T_{total}$) was calculated, as shown in Figure 4c. The minimum specular


dx.doi.org/10.1021/am405865w | ACS Appl. Mater. Interfaces 2014, 6, 6164−6169

transmittance that also represented the zeroth-order diffraction wavelength red shifted with increased period. Note that the peaks and dips in the haze measurements will be red shifted and eliminated, respectively, after completion of the device processes (i.e., after the deposition of ITO, polymers, and metals that had higher refractive indices) because of the photons are now entering into dense media instead of the air. The calculated haze factors of a completed device, assuming a polymer layer with a refractive index of 2.0 deposited on the patterned ITO electrode, are also shown in parallel in Figure 4c. Those haze factors were calculated using a rigorous coupled wave analysis (RCWA) model. The RCWA approach was employed to analyze the optical diffraction and transmission properties of the nanoscale structures and to solve the Maxwell's equations in a periodic medium after applying the field and permittivity. In this work, a commercial implementation of the three-dimensional RCWA (DiffractMod, Rsoft Corp.) was used. As shown in Figure 4c, all structured surfaces showed a higher haze factor values than the flat one in the visible range, which explained the increased $J_{sc}$ in the $J-V$ measurements. The effects of the high haze factors were also reflected in the EQE measurements.

The different degrees of enhancements were subsequently considered with structures of different periods in the $J_{sc}$ and EQE for our OPV devices. Figure 4d shows a schematic of the setup for measuring the diffraction angles. The transmitted diffraction patterns through the structured samples were projected onto a white screen using a collimated laser beam operated at 488 nm. As aforementioned, the diffraction angles increased as the periods were reduced. By measuring the distance from the laser center spot (i.e., the zeroth-order diffraction) to the hexagonal-shaped diffraction points (Figure 4d), the diffraction angles were determined. The diffraction angles of the hexagonal-shaped diffraction points, at an incident light of 488 nm were 68.2, 45.0, and 26.6° for periods of 600, 800, and 1200 nm, respectively. This finding showed that the diffraction patterns produced by structures of short period had larger diffraction angles than those produced by longer periods. The larger diffraction angles provided an elongated optical path for incident light and made the light reach the back electrode with larger angles. Thus, the reflected light coupled with the guiding modes with the help of the back reflector and crossed the active layer at a larger angle on its way back. This phenomenon increased the path for absorption and concentrated the light in the absorber. Note that the effect of the large angle diffraction significantly benefited the long wavelength light and resulted in the best EQE performance near the absorption band edge for the 600 nm period structure (Figure 3b). The above arguments also explained why devices with structures of the 1200 nm period that had a high haze factor (Figure 4c) showed only enhanced $J_{sc}$ and EQE comparable to devices with 600 nm period structures. We speculate that the higher haze from the 1200 nm period is due to the larger height contrast produced by the spin-coating process of the second SU-8 layer. It was the trade-off between two factors, the highly diffused light, and the larger diffraction angle that led to the higher performance of the OPV device with a surface structure of an 800 nm period than the others.

In summary, techniques that can enable efficient optical absorption in films thinner than the optical absorption length must be developed. For this purpose, surface structures such as periodic patterns or rough surfaces can increase the effective optical path of incident light inside the absorbing materials by light trapping or scattering. A conductive and transparent substrate with periodic surface structures was used. The waveguide theory predicts that periodic structures should outperform random textures, because they avoid scattering into lossy radiation channels.[30] On the other hand, the periodic structures which have uniform aspect ratio would benefit following materials such as ITO and polymer coatings with uniform thickness. This substrate provided high light diffusion and high diffraction angles. The surface structures were fabricated by UV-curing nanoimprint lithography to achieve uniform and conformal coating of organic materials on top of the nanostructured surface. The organic solar cells with deposited active layer of P3HT:PCBM onto the structured substrate showed improved PCE of 3.92% and $J_{sc}$ of 10.76 mA/cm$^2$. The improvement in device performance was attributed to the elongated path and enhanced light absorption caused by the structures on the ITO electrodes. Our research provided an effective, simple, scalable, and cost-effective method of further enhancing thin film solar cell efficiency using structured electrodes with light trapping.

## AUTHOR INFORMATION


### Corresponding Author

*E-mail: kwsun@mail.nctu.edu.tw.


### Author Contributions

The manuscript was written through contributions of all authors. All authors have given approval to the final version of the manuscript.

### Notes

The authors declare no competing financial interest.

## ACKNOWLEDGMENTS

This work is supported by the Ministry of Science and Technology of the Republic of China (Contract NSC 102-2112-M-009-011-MY3) and the Approaching Top University (ATU) Program of the Ministry of Education of the Republic of China.

## REFERENCES


(1) Chen, H. Y.; Hou, J.; Zhang, S.; Liang, Y.; Yang, G.; Yang, Y.; Yu, L.; Wu, Y.; Li, G. Polymer Solar Cells with Enhanced Open-Circuit Voltage and Efficiency. *Nat. Photonics* **2009**, *3*, 649−653.

(2) Liang, Y.; Xu, Z.; Xia, J.; Tsai, S. T.; Wu, Y.; Li, G.; Ray, C.; Yu, L. For the Bright Future−Bulk Heterojunction Polymer Solar Cells with Power Conversion Efficiency of 7.4%. *Adv. Mater.* **2010**, *22*, E135−E138.

(3) He, Z.; Zhong, C.; Huang, X.; Wong, W. Y.; Wu, H.; Chen, L.; Su, S.; Cao, Y. Simultaneous Enhancement of Open-Circuit Voltage, Short-Circuit Current Density, and Fill Factor in Polymer Solar Cells. *Adv. Mater.* **2011**, *23*, 4636−4643.

(4) Chattopadhyay, S.; Huang, Y.F.; Jen, Y.J.; Ganguly, A.; Chen, K.H.; Chen, L.C. Anti-Reflecting and Photonic Nanostructures. *Mater. Sci. Eng., R* **2010**, *69*, 1−35.

(5) Li, Y.; Zhang, J.; Yang, B. Antireflective Surfaces Based on Biomimetic Nanopillared Arrays. *Nano Today* **2010**, *5*, 117−127.

(6) Garnett, E.; Yang, P. Light Trapping in Silicon Nanowire Solar Cells. *Nano Lett.* **2010**, *10*, 1082−1087.

(7) Lu, Y.; Lal, A. High-Efficiency Ordered Silicon Nano-Conical-Frustum Array Solar Cells by Self-Powered Parallel Electron Lithography. *Nano Lett.* **2010**, *10*, 4651−4656.

(8) Ferry, V. E.; Verschuuren, M. A.; Claire van Lare, M.; Schropp, R. E. I.; Harry, A. A.; Albert, P. Optimized Spatial Correlations for Broadband Light Trapping Nanopatterns in High Efficiency Ultrathin Film a-Si:H Solar Cells. *Nano Lett.* **2011**, *11*, 4239−4245.

(9) Chen, J. Y.; Chang, W. L.; Huang, C. K.; Sun, K. W. Biomimetic Nanostructured Antireflection Coating and Its Application on Crystalline Silicon Solar Cells. *Opt. Express* **2011**, *19*, 14411−14419.
(10) He, L.; Jiang, C.; Wang, H.; Lai, D.; Rusli, Si Nanowires Organic Semiconductor Hybrid Heterojunction Solar Cells Toward 10% Efficiency. *ACS Appl. Mater. Interfaces* **2012**, *4*, 1704−1708.
(11) Jeong, S.; Garnett, E. C.; Wang, S.; Yu, Z.; Fan, S.; Brongersma, M. L.; McGehee, M. D.; Cui, Y. Hybrid Silicon Nanocone-Polymer Solar Cells. *Nano Lett.* **2012**, *12*, 971−2976.
(12) Nalwa, K. S.; Park, J. M.; Ho, K. M.; Chaudhary, S. On Realizing Higher Efficiency Polymer Solar Cells Using a Textured Substrate Platform. *Adv. Mater.* **2011**, *23*, 112−116.
(13) Hsu, M. H.; Yu, P.; Huang, J. H.; Chang, C. H.; Wu, C. W.; Cheng, Y. C.; Chu, C. W. Balanced Carrier Transport in Organic Solar Cells Employing Embedded Indium-Tin-Oxide Nanoelectrodes. *Appl. Phys. Lett.* **2011**, *98*, 073308.
(14) Müller-Meskamp, L.; Kim, Y. H.; Roch, T. S.; Scholz, R.; Eckardt, S.; Leo, K.; Lasagni, A. F. Efficiency Enhancement of Organic Solar Cells by Fabricating Periodic Surface Textures Using Direct Laser Interference Patterning. *Adv. Mater.* **2012**, *24*, 906−910.
(15) Hu, Z.; Zhang, J.; Zhao, Y. J. Effect of Textured Electrodes with Light-Trapping on Performance of Polymer Solar Cells. *J. Appl. Phys.* **2012**, *111*, 104516.
(16) Chou, W. Y.; Chang, J.; Yen, C. T.; Tang, F. C.; Cheng, H. L.; Chang, M. H.; Hsu, S. L. C.; Chen, J. S.; Lee, Y. C. Nanoimprinting-Induced Efficiency Enhancement in Organic Solar Cells. *Appl. Phys. Lett.* **2011**, *99*, 183108.
(17) Yang, Y.; Lee, K.; Mielczarek, K.; Hu, W.; Zakhidov, A. Nanoimprint of Dehydrated PEDOT:PSS for Organic Photovoltaics. *Nanotechnology* **2011**, *22*, 485301.
(18) Zhu, X.; Choy, W. C. H.; Xie, F.; Duan, C.; Wang, C.; He, W.; Huang, F.; Cao, Y. A Study of Optical Properties Enhancement in Low-Band Gap Polymer Solar Cells with Embedded PEDOT:PSS Gratings. *Sol. Energy Mater. Sol. Cells* **2012**, *99*, 327−332.
(19) Li, K.; Zhen, H.; Huang, Z.; Li, G.; Liu, X. Embedded Surface Relief Gratings by a Simple Method to Improve Absorption and Electrical Properties of Polymer Solar Cells. *ACS Appl. Mater. Interfaces* **2012**, *4*, 4393−4397.
(20) Na, S. I.; Kim, S. S.; Jo, J.; Oh, S. H.; Kim, J.; Kim, D. Y. Efficient Polymer Solar Cells with Surface Relief Gratings Fabricated by Simple Soft Lithography. *Adv. Funct. Mater.* **2008**, *18*, 3956−3963.
(21) He, X.; Gao, F.; Tu, G.; Hasko, D. G.; Hüttner, S.; Greenham, N. C.; Steiner, U.; Friend, R. H.; Huck, W. T. S. Formation of Well-Ordered Heterojunctions in Polymer:PCBM Photovoltaic Devices. *Adv. Funct. Mater.* **2011**, *21*, 139−146.
(22) Chen, D.; Zhao, W.; Russell, T. P. P3HT Nanopillars for Organic Photovoltaic Devices Nanoimprinted by AAO Templates. *ACS Nano* **2012**, *6*, 1479−1485.
(23) Li, X.; Choy, W. C. H.; Huo, L.; Xie, F.; Sha, W. E. I.; Ding, B.; Guo, X.; Li, Y.; Hou, J.; You, J.; Yang, Y. Dual Plasmonic Nanostructures for High Performance Inverted Organic Solar Cells. *Adv. Mater.* **2012**, *24*, 3046−3052.
(24) Li, X.H.; Sha, W. E. I.; Choy, W. C. H.; Fung, D. D. S.; Xie, F. X. Efficient Inverted Polymer Solar Cells with Directly Patterned Active Layer and Silver Back Grating. *J. Phys. Chem. C* **2012**, *116*, 7200−7206.
(25) Pandey, A. K.; Aljada, M.; Velusamy, M.; Burn, P. L.; Meredith, P. Nanostructured, Active Organic−Metal Junctions for Highly Efficient Charge Generation and Extraction in Polymer-Fullerene Solar Cells. *Adv. Mater.* **2012**, *24*, 1055−1061.
(26) Guo, L.J. Nanoimprint Lithography: Methods and Material Requirements. *Adv. Mater.* **2007**, *19*, 495−513.
(27) Schift, H. J. Nanoimprint Lithography: An Old Story in Modern Times? A Review. *J. Vac. Sci. Technol., B* **2008**, *26*, 458−480.
(28) Hsu, C. M.; Battaglia, C.; Pahud, C.; Ruan, Z.; Haug, F.J.; Fan, S.; Ballif, C.; Cui, Y. High-Efficiency Amorphous Silicon Solar Cell on a Periodic Nanocone Back Reflector. *Adv. Energy Mater.* **2012**, *2*, 628−633.
(29) Dang, M.T.; Hirsch, L.; Wantz, G. P3HT:PCBM, Best Seller in Polymer Photovoltaic Research. *Adv. Mater.* **2011**, *23*, 3597−3602.
(30) Battaglia, C.; Hsu, C.M.; Söderström, K.; Escarré, J.; Haug, F.J.; Charrière, M.; Boccard, M.; Despeisse, M.; Alexander, D. T. L.; Cantoni, M.; Cui, Y.; Ballif, C. Light Trapping in Solar Cells: Can Periodic Beat Random? *ACS Nano* **2012**, *6*, 2790−2797.